Applied Surface Science 388 (2016) 252–258

Contents lists available at ScienceDirect

Applied Surface Science

journal homepage: www.elsevier.com/locate/apsusc

Effect of hydrogen uptake on the electrochemical corrosion of N18 zircaloy under gamma irradiation

Z.Y. Xin [a], Y.H. Ling [a,*], Y.K. Bai [a], C. Zeng [a], S. Wang [a], J.C. Clara [b]

[a] Lab of Advanced Materials, School of Materials Sciences and Engineering, Tsinghua University, Beijing 100084, China
[b] Department of Chemistry, University of Western Ontario, London N6A 5B7, Ontario, Canada

ARTICLE INFO

Article history:
Received 14 October 2015
Received in revised form 18 January 2016
Accepted 18 January 2016
Available online 21 January 2016

Keywords:
Zircaloy
Hydrogen permeation
Gamma irradiation
Corrosion

ABSTRACT

It has been well recognized that dramatic hydrogen uptake occurred in zircaloy after kinetic transition and porous structure was observed subsequently due to phase transformation of tetragonal to monoclinic zirconia. Therefore, how hydrogen solute and gamma-induced capillary-embedded hydrolysis influence the corrosion of zircaloy is an intriguing issue. In this work, the effect of hydrogen uptake and gamma irradiation on corrosion of N18 zircaloy was studied. Raman spectra and atomic force microscopy (AFM) were employed to analyse phase structure and surface morphology. Potentiodynamic polarization and electrochemical impedance spectroscopy were utilized to qualitatively evaluate the electron transfer properties of the oxide film formed on the zircaloy surface after corrosion. The depth profile and surface chemical states of involving elements were analysed by auger electron spectroscopy (AES) and X-ray photoelectron spectroscopy (XPS), respectively. It was found that hydrogen permeation can decline the integrity and impedance semicircle of the oxide films, the more the hydrogen uptake is; the smaller magnitude of impedance will be. In view of the gamma irradiation, it is demonstrated that it promotes the corrosion rate slightly. Based on the irradiation theory and existing phenomena, the underlying mechanism is proposed.

1. Introduction

Zirconium alloys (zircaloys) are widely used as the fuel cladding materials for current PWR and BWR nuclear reactors due to its low absorption cross section for neutrons, good mechanical properties and high resistance to corrosion. The harsh work conditions, however, bring severe waterside corrosion on zircaloys, including hydrothermal oxidation, hydrogen uptake as well as irradiation damage. The current zircaloys (including Zr-2, Zr-4 and beyond) will not be robust enough against these more aggressive service conditions. By alloying zirconium, both the mechanical and corrosion properties can be greatly improved. As a result, replacing the traditional zircaloy like Zr-4 with novel types is of priority and has achieved great success, including Zirlo in Westinghouse, M5 in France and N18 in China.

The integrity of ZrO_2 passive film is of significance to its protective character. Irradiation corrosion of zircaloy is an important issue in both safety and economic aspects. Thelack of understanding of the process and corresponding mechanism, however, restricted the research and development of new zircaloy. The corrosion resistance of the oxide film formed on zircaloy is strongly influenced by hydrogen absorption and the microstructure change under gamma irradiation. The primary corrosion products of ZrO_2 existed in mostly two types, i.e. the compact tetragonal phase and the strain-induced loose monoclinic phase [1]. Additionally, it has been reported that hydrogen uptake during the corrosion of zircaloy is a very local process, and always occurred at the sites with cracks or small holes on the oxide surface, therefore, a compact zirconia film can retard the corrosion process. Besides, defects induced by hydrogen uptake can conversely lead to a degradation of the oxides, causing an elevated corrosion rate [2–4]. As for the effect of gamma irradiation, it is well explicated that the corrosion rate is positive-correlated with the carrier concentration. It is due to the irradiation induced ionization effect that the carrier concentration in the oxides multiplies and thus leads to a higher corrosion rate [5–9]. Also, the formation of hydrogen peroxide during gamma irradiation has been reported to be associated with the increase of corrosion rate as well [10,11]. In spite of the extensive studies on the individual effect of hydrogen uptake and gamma irradiation on the corrosion rate of zircaloys, the research on the coupling effect of them is still scant.

* Corresponding author. Tel.: +86 1062772856.
E-mail address: yhling@mail.tsinghua.edu.cn (Y.H. Ling).

http://dx.doi.org/10.1016/j.apsusc.2016.01.158
0169-4332/

In our present work, the effect of both hydrogen absorption and irradiation on the corrosion behaviour of N18 zircaloy was investigated. The phase structure, surface morphology, element depth profile and involving valence states were analysed by comprehensive surface analysing techniques. We found that hydrogen permeation can promote the corrosion rate of the zircaloy and gamma irradiation further accelerates the growth rate of the oxide film.

2. Experimental

2.1. Sample preparation

The N18 zircaloys used in this work were provided by Nuclear Power Institute of China (NPIC). The samples were cut into 10 mm × 10 mm with 1 mm in thickness and the chemical composition was shown in Table 1. All the samples were polished to 7000# SiC waterproof abrasive paper and 0.5 μm diamond paste to attain a mirror-like surface. Before hydrogen permeation, all the specimens were ultrasonically rinsed with acetone and ethyl alcohol and then with deionized water, respectively.

2.2. Hydrogen charging and hydrothermal oxidation

In order to simulate the PWR work condition, the electrochemically cathodic charging was applied on an electrochemical workstation in the electrolyte of 0.1 M H_3BO_3 + 0.01 M LiOH aqueous solution at room temperature with duration of 30 min, and current density was 1 mA/cm^2, 5 mA/cm^2 and 10 mA/cm^2, respectively, which is equivalent to total electric charge of 1.8 C, 9 C and 18 C, respectively. Hydrothermal oxidation of as-charged N18 zircaloy samples was conducted in a homemade static autoclave with simulating water chemistry in primary loops of PWR (a deoxygenated aqueous B-Li solution consisting of 0.1 M H_3BO_3 and 0.01 M LiOH), at 200 °C for 4 h. Samples were irradiated by exposing on the ^{60}Co gamma environment to imitate the in-pile ionizing radiation. The gamma irradiation was carried out in an MDS Nordion Gammacell 220 Excel Cobalt-60 irradiator at University of Western Ontario. The radiation absorption dose rate was 3.1 kGy h^{-1} (where 1 Gy is 1 J kg^{-1}). Samples were exposed to gamma irradiation for 4 hours, and the temperature was kept at 200 °C. Note that for safety consideration, our preliminary experiments select a much lower temperature than that in reactor (about 300 °C).

2.3. Surface and electrochemical characterization

Raman spectrometer (Lab RAM HR Evolution, HORIBA Scientific, Japan) using argon ion laser with 532 nm excitation wavelength was used to identify the phase structure of the oxide film formed on N18 zircaloy. The surface morphologies of the oxide film were observed by atomic force microscopy (AFM, NTEGRA Solaris, NT-MDT, Russia) with a spotting area of 100 μm^2. The distribution of elements in oxide film as a function of depth was detected by auger electron spectroscopy (AES, PHI-700 Scanning Auger Microscope spectrometer, ULVAC-PHI, Japan) using Ar^+ ion gun and SiO_2 was used as the reference in the AES test. X-ray photoelectron spectroscopy (XPS, ESCALAB 250Xi X-ray Photoelectron Spectrometer, Thermo Fisher Scientific, USA) was employed to analyse the chemical state and the change of composition of surface after hydrogen permeation, and a monochromated Al source was used in the XPS spectra collection. The C1s peak for adventitious hydrocarbon at 284.60 eV was referenced by all spectra to correct the binding energy shift.

Table 1
Chemical composition of N18 zircaloy.

Element (wt.%)	Sn	Nb	Fe	Cr	O	Zr
Content	1.05	0.28	0.31	0.10	0.09	Bal.

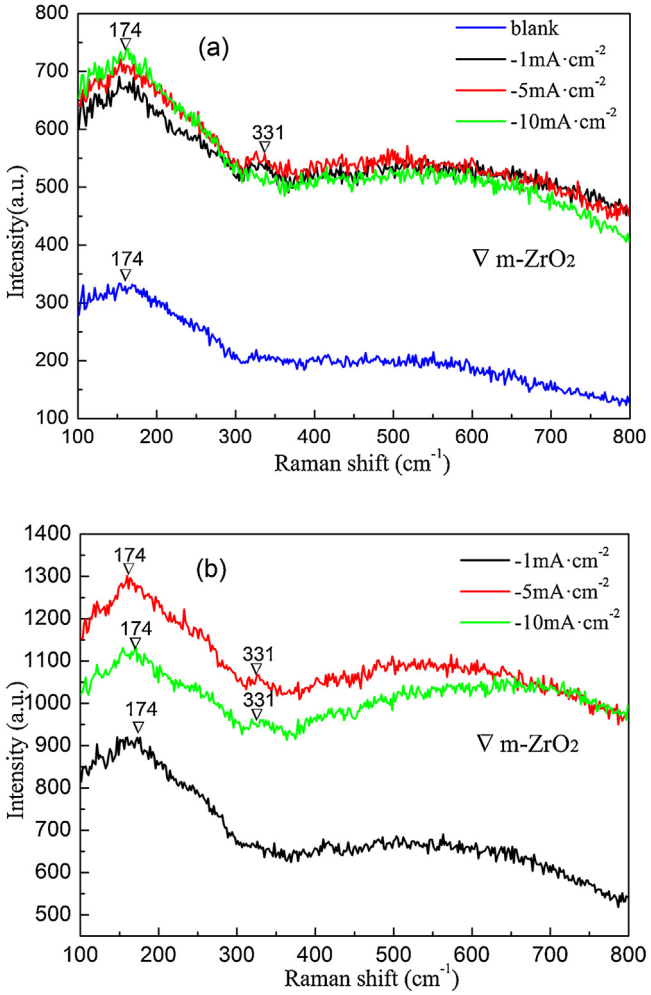

Fig. 1. Raman spectra of the oxide films without (a) and with (b) irradiation.

Electrochemical tests, including the open circuit potential (OCP), electrochemical impedance spectroscopy (EIS) and potentiodynamic polarization were performed on an electrochemical workstation (IM6E, ZAHNER, Germany). The configuration used was a three-electrode system with saturated calomel electrode (SCE) as reference electrode and platinum electrode being counter electrode. All the measurements were carried out in 0.1 M H_3BO_3 + 0.01 M LiOH solution at room temperature. The OCP was first measured for 1 hour. Then the EIS test was conducted with a frequency from 1 M Hz to 10 m Hz at the excitation voltage of 10 mV. Potentiodynamic polarization curves were recorded from a potential 0.1 V negative than the OCP to a potential 0.1 positive than it with a scan rate of 0.1667 mV/s, and a Xenon lamp with a power intensity of 100 Mw/cm^2 was implemented as simulated solar light.

3. Results and discussion

3.1. Phase and morphology

In order to confirm the phase composition of the oxide film, Raman spectra were utilized. Fig. 1(a) shows two main peaks at 174 cm^{-1} and 331 cm^{-1} which is in agreement with the

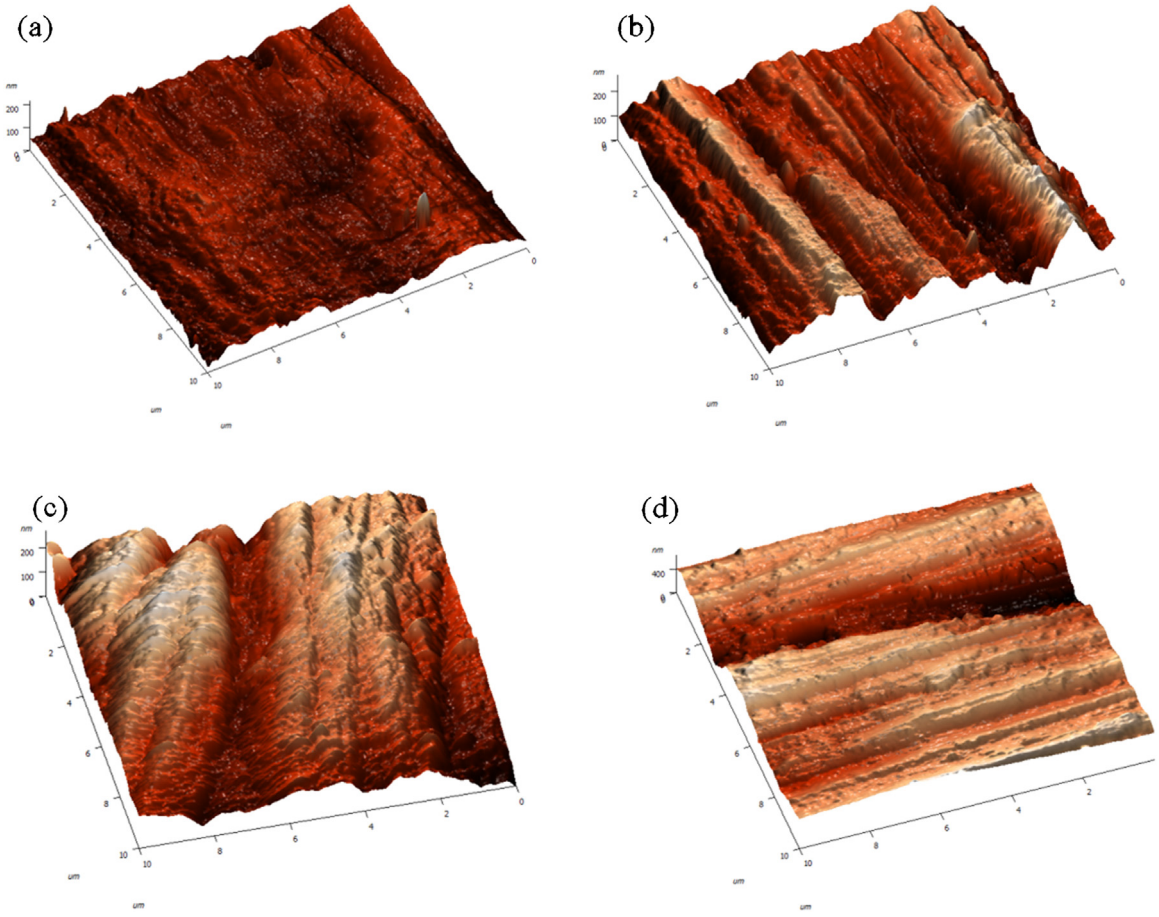

Fig. 2. AFM morphologies for oxides without irradiation using charging current of 0 mA/cm^2 (a) and −5 mA/cm^2 (b) and oxides with irradiation using charging current of −1 mA/cm^2 (c) and −5 mA/cm^2 (d).

characteristics of monoclinic zirconia in the literature. From Fig. 1(b), it is clear that the predominant phase in the oxides remains almost unchanged. Therefore, the oxide films in our work are mainly composed of monoclinic ZrO_2.

The AFM images for oxide films without irradiation are shown in Fig. 2(a–b). Compared to the oxide film using a −5 mA cm^2 charging current density, the blank one is relatively smoother with average roughness of 14 nm. It can be inferred that the elevated oxidation rate, partly because of the larger charging density, results in the much more uneven surface, i.e. an average roughness of 35 nm, 1.5 folds higher than that of blank one. Surface roughness of oxides with gamma irradiation increases significantly (Fig. 2(c–d)). For oxides with gamma irradiation using a −1 mA/cm^2 and −5 mA/cm^2 charging current density, the surface roughness is around 38 nm and 74 nm, respectively. Similarly, the roughness of the oxides using a larger charging current (−5 mA/cm^2) is much higher than that using a smaller charging current (−5 mA/cm^2), in accordance with the roughness results without irradiation. In addition, comparing the surface morphologies of oxides using the same charging current (−5 mA/cm^2) without and with gamma irradiation, it can be inferred that gamma irradiation further promotes the growth rate of the oxides [12,13], leading to a much higher roughness 74 nm versus the roughness of 38 nm without irradiation.

3.2. Potentiodynamic polarization

Fig. 3 shows the change of logarithm current with electrode potential. By fitting the potentiodynamic polarization curves one can get the self-corrosion current (i_{corr}) and self-corrosion potential

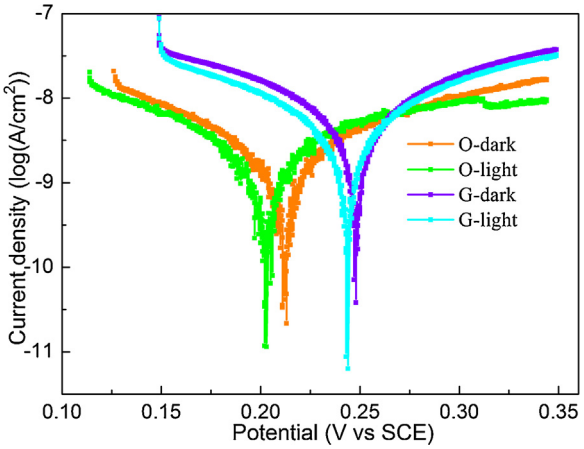

Fig. 3. The potentiodynamic polarization curves of oxide films on surface of N18 zircaloy with or without irradiation. Note that all samples are cathodic charged with 5 mA/cm^2 prior to hydrothermal oxidation. The letter O refers to without rad. and G refers to with gamma rad.

(E_{corr}). As shown in Table 2, it is clear that with gamma irradiation, both the self-corrosion potential and current increased. The increase of E_{corr} might be related to the thickening of oxide film under gamma irradiation, but the same change of i_{corr} may indicate that the structure of the oxide films are not that dense, as can be seem from the R_p. The reasons for this phenomenon may be that gamma irradiation introduces more defects into the oxide film and thus promotes the growth rate of the oxides. It should be pointed

Table 2
Electrochemical parameters of samples extracted from Fig. 3.

Charging current (mA/cm^2)	Hydrothermal oxidation	Xe light illumination	i_{corr} (A/cm^2)	E_{corr} (V)
−5	No rad.	off	1.3230E-09	0.212
−5	Rad.	off	5.1710E-09	0.248
−5	No rad.	on	1.4240E-09	0.202
−5	Rad.	on	5.5923E-09	0.244

out that both for the oxides with and without gamma irradiation, the self-corrosion potentials shift negatively and the current densities increase with illumination, compared to those without illumination. Electron-hole pairs are generated in large amounts on the electrode surface because of the excitation of electrons stimulated by the illuminating of Xe light, whose energy is supposed to be higher than that of the band gap, and then conduction band bends, which causes more efficient charge separation and hence increases the photocurrent [14]. As shown in Fig. 3, under the illumination of Xe lamp, the self-corrosion current (i_{corr}) of N18 zircaloy increases while the self-corrosion potential (E_{corr}) decreases, probably due to the N-type semiconductor character of the oxide films formed on N18.

3.3. Electrochemical impedance spectroscopy

The oxide microstructure usually changes with the impedance variation. Fig. 4 and Fig. 5 depict the Nyquist and Bode plots for oxides without and with irradiation respectively.

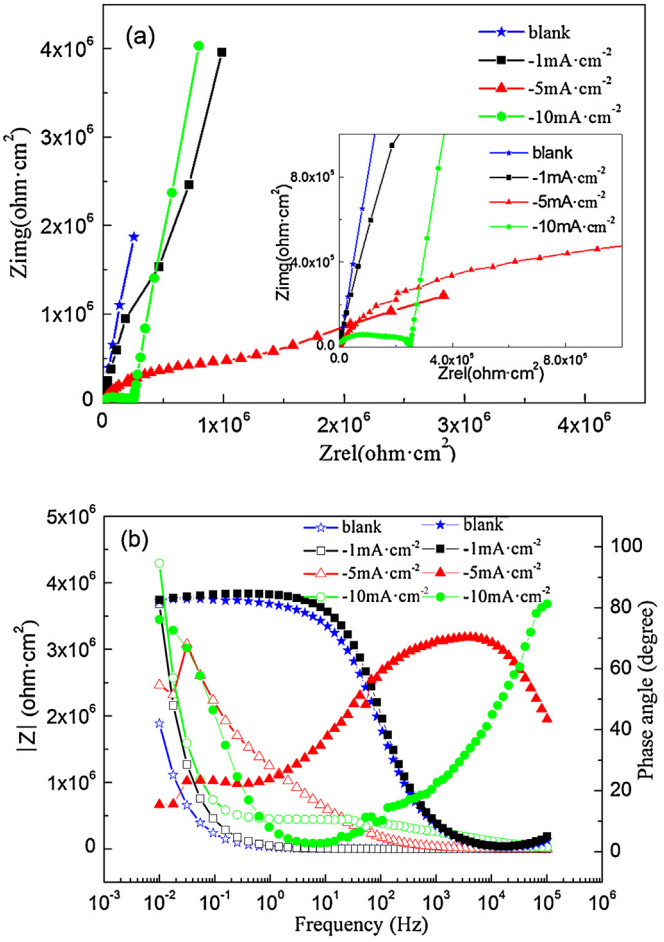

Fig. 4. The Nyquist plots (a) and Bode plot (b) of oxide film on N18 zircaloy without irradiation. The inset in Nyquist plot was magnification of high frequency scan range.

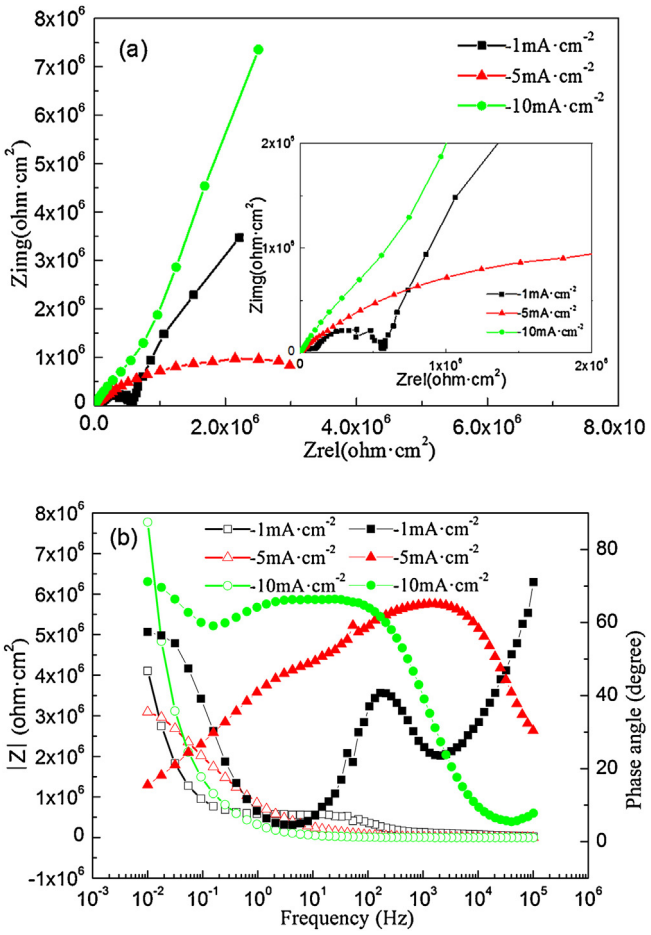

Fig. 5. The Nyquist plots (a) and Bode plot (b) of oxide film formed on N18 zircaloy with irradiation. The inset in Nyquist plot was magnification of high frequency range.

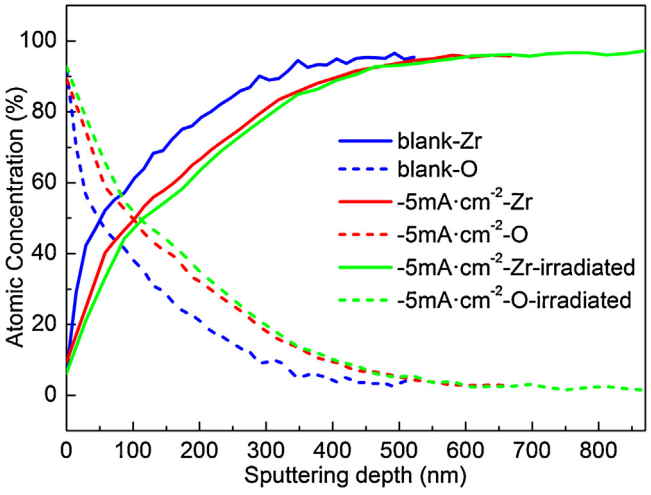

Fig. 6. Depth profiles of oxides using charging current density of 0 mA/cm^2 and −5 mA/cm^2 without irradiation, and using −5 mA/cm^2 with irradiation.

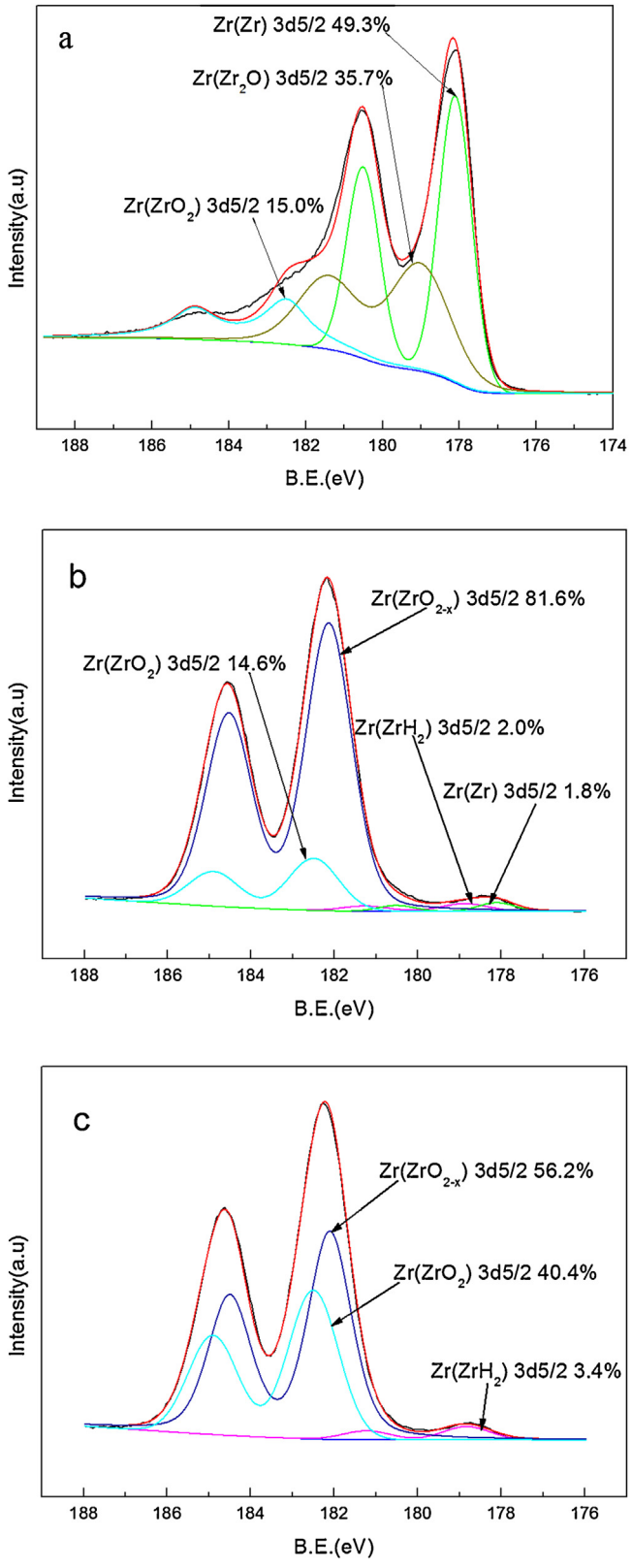

Fig. 7. XPS spectra of Zr3d for N18 zircaloy samples with hydrogen charging current of 0 mA/cm^2 (a), −5 mA/cm^2 (b) and −10 mA/cm^2 (c).

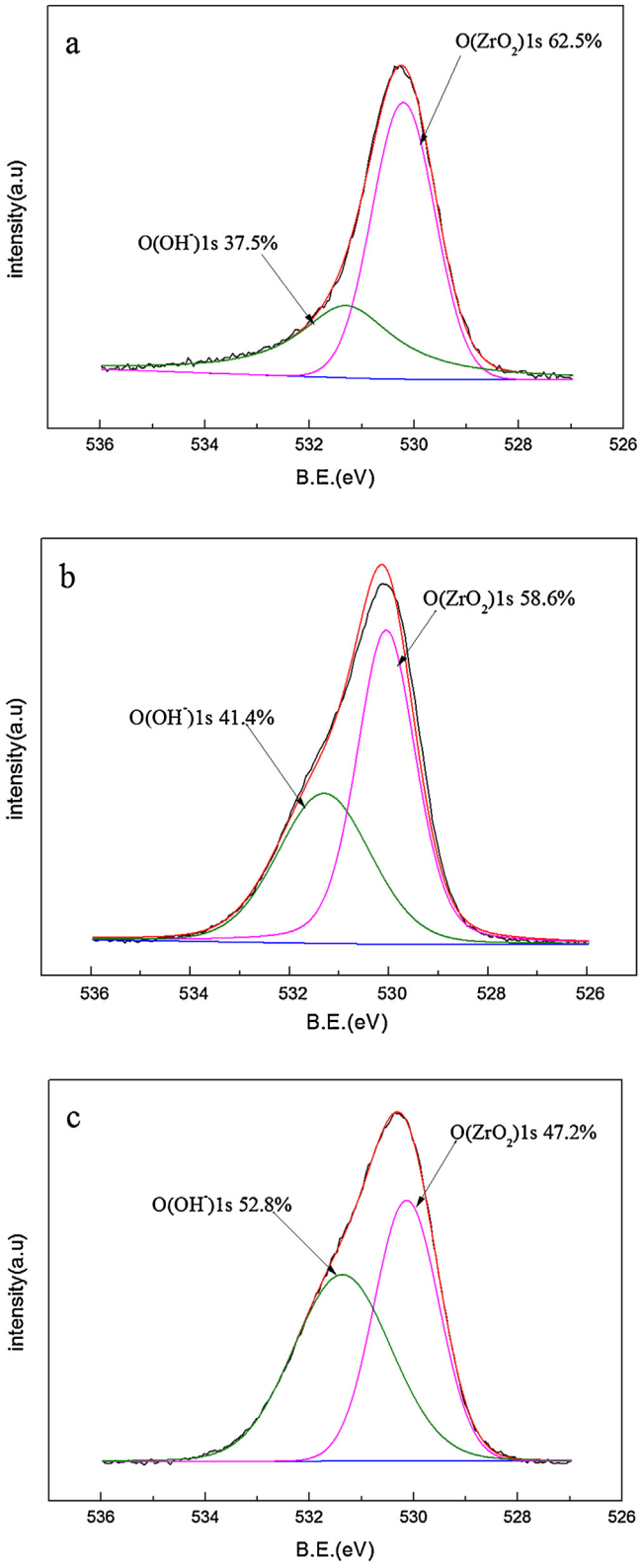

Fig. 8. XPS spectra of O1s for N18 zircaloy samples with hydrogen charging current of 0 mA/cm^2 (a), −5 mA/cm^2 (b) and −10 mA/cm^2 (c).

As shown in Fig. 4, the increase of charging current density leads to the augmentation of impedance magnitude. However, compared to the blank sample, the impedance semicircles of samples after hydrogen permeation bend as shown in Fig. 4(a), and the phase angles at low frequencies (f < 1 Hz) decrease apparently, which indicates a loss of integrity of the oxides. For an ideal 'integrity', the phase angle should be 90°, otherwise the smaller the phase angle is, and the less integrity the oxides will be of. The degradation of the oxide with hydrogen permeation probably results from the abundant additional defects introduced by the

Table 3
Thickness and OCP values of the passive ZrO_2 films.

Method of oxidation	Direct hydrothermal				γ-irradiation		
Hydrogen permeation current (mA cm^{-2})	0	−1	−5	−10	−1	−5	−10
Thickness of films/nm	4.3	44.6	210.2	223.6	30.8	47.9	101.6
OCP values (V)	0.143	0.226	0.215	0.255	0.129	0.156	0.247

penetrating hydrogen in it [15,16]. However, it should be mentioned that unlike other samples with hydrogen permeation, the sample using a −10 mA cm^{-2} charging current shows an increase in the impedance magnitude. It is widely accepted that the hydrogen solubility has an upper limit. The excessive hydrogen therefore may react with the zircaloy matrix and form a layer of zirconium hydride, leading to the increase of impedance magnitude and rising of two slopes in the phase angle plot.

In comparison of Fig. 4 and Fig. 5, it is obvious that the impedance magnitude and phase angle at low frequencies of oxides with irradiation are much lower than that without irradiation. To the best of our knowledge, gamma irradiation can arouse the ionization of water and oxides, along with ensuing accretion of massive OH^- and irradiation-induced defects. The conductivity consequently accrues, making it easier for carriers to diffuse via these newly-formed defective shortcuts [17].

The thickness of dense layer in the oxides, L_{ss}, can be estimated via the parallel plate approximation:

$$\mathrm{Lss} = \frac{\varepsilon\varepsilon_0}{C}$$

C is obtained from $C = -1/wZ''$, where ε (vacuum permittivity) equals 8.85×10^{14} F/cm and ε_0 is the dielectric constant as being 20–31.5 for ZrO_2 [18]. Table 3 shows the thickness of the dense layer and OCP values of all the samples. It also can be seen that the dense layer becomes thicker with the increase of hydrogen charging current, indicating that hydrogen permeation promotes the growth of oxide film. Nevertheless, due to the irradiation-induced defects, the thicknesses of dense layer with gamma irradiation in oxide film are lower than those samples without irradiation (as seen in Table 3).

3.4. Elements depth profile

To unravel the effect of hydrogen permeation and gamma irradiation on the corrosion rate, AES depth profiles were therefore plotted in Fig. 6. Generally, the oxide thickness can be estimated by the depth profile according to the distance between the starting point and the plateau where O concentration reaches a minimum value approximate to 0%. Therefore, the thickness of oxides, indirectly derived from the depth profiles, can be used to compare and reflect the oxidation rate. The estimated oxide thickness of the blank sample (0 mA cm^{-2} without irradiation) is 522 nm, while the oxide thickness is 667 and 870 nm for samples using the same charging current (0 mA cm^{-2}) without and with irradiation, respectively. Furthermore, the meeting points of Zr and O shift to higher sputtering depth values with larger hydrogen permeation current and gamma irradiation. The AES depth profiles are well consistent with the AFM and EIS results, confirming that the hydrogen permeation and gamma irradiation can both accelerate the corrosion rate.

3.5. Corrosion mechanism analysis

X-ray photoelectron spectroscopy (XPS) was applied to investigate the chemical state of Zr3d and O1s prior to hydrothermal oxidation with different hydrogen charging current densities. Fig. 7 shows the fitting results of the Zr3d spectra. The spin-orbit splitting between Zr3d5/2 and Zr3d3/2 peak value is fixed as 2.4 eV. For blank sample with 0 mA cm^{-2} charging current density, the Zr3d spectra can be decomposed into species pertaining to Zr, Zr_2O and ZrO_2, respectively, and the pertinent percentage is also provided in Fig. 7. After hydrogen permeation, the Zr3d component attributed to ZrH_2 arises in Zr3d spectra. Since the solubility of H in Zr is at a considerable low level of 10^{-4} at.% at room temperature. Thus the excess hydrogen uptake will react with the zircaloy matrix and

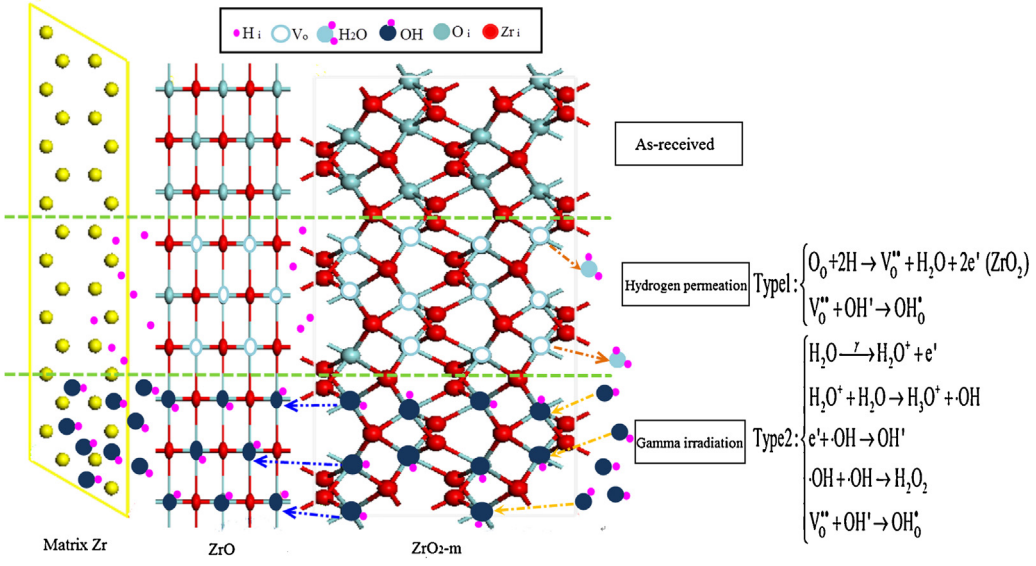

Fig. 9. Schematic illustration of the mechanism of hydrogen permeation and gamma irradiation on the corrosion behavior of N18 zircaloy.

probably form a small amount of hydrides [19]. As shown in Fig. 7(b) and (c), when the charging current density rises, there is an obvious increase in the amount of ZrO_2, and yet a distinct decrease in the amount of Zr. Also, there is a minute increase of the amount of ZrH_2. The binding energies measured by Nishino, Akhiani and Corbett were taken as reference [20–22].

As is shown in the Fig. 8(a–c), the O1s spectra for blank sample and samples with hydrogen permeation are all composed of two peaks, of which peak at 530.1 eV is assigned to ZrO_2 and the other peak at 531.3 eV is probably attributed to hydroxyl species, such as OH^- [23–26]. Hence, it can be confirmed that hydrogen penetrates into zircaloy through cathodic hydrogen charging method. Fig. 8 reveals that the percentage of hydroxyl species is augmented with the enhancement of charging current. It is probably because the absorbed hydrogen on the surface reacts with oxygen that the amount of hydroxyl species proliferates rapidly. On the other hand, the oxygen vacancies formed during the reduction reaction can combine with hydrogen to form hydrogen defect, which provides fast-diffusion paths for hydrogen. It is therefore inferred that the effect of hydrogen permeation probably stems from the arising and accretion of the hydroxyl species OH^-.

Based on the acknowledged theory and existing phenomena, the possible mechanism was proposed and schematic illustrated in Fig. 9. The reactions occurring under the influence of hydrogen permeation and gamma irradiation can, largely, be divided into two types.

Type 1 includes the formation of oxygen vacancies and the recombination of OH^- with oxygen vacancy. Large amount of oxygen vacancies formed due to the reduction reaction between hydrogen and oxides, and then OH^- reacts with oxygen vacancies and leads to the multiply of hydrogen defects, thus hydrogen penetration is promoted with the oxidation process significantly accelerated.

Type 2 reveals the water radiolysis processes and the formation of hydroxide radicals. As shown in Fig. 9, massive OH^- derived from the decomposition effect of H_2O under gamma irradiation and eventually promotes the corrosion rate [27,28], similar to the process shown in Type 1. Moreover, hydrogen peroxide generated during the decomposition process is a kind of strong oxidant due to its active chemical property, and thus the oxidation process is further sped up.

4. Conclusion

In summary, the effect of hydrogen permeation and gamma irradiation on the corrosion behaviour of N18 zircaloy was investigated in this work. Based on the integrated analysis techniques concerning phase composition, surface morphology and semiconductor properties, preliminary results were attained. It can be concluded that:

Hydrogen permeation promotes the corrosion rate of N18 zircaloy. It is probably the proliferation of defects induced by the hydrogen uptake, such as oxygen vacancies and hydroxyl species, which leads to the significant increase of corrosion rate.

Gamma irradiation can also accelerate the corrosion rate. The ionization of water, the augmentation of hydrogen defects induced by irradiation and ensuing better conductivity of the oxides are considered to account for the irradiation-promoted corrosion process.

Acknowledgments

This research was funded by the National Basic Research Program of China (973 Program) under grant No. 2011CB61050, the NSAF program (No.U1430118), the Reactor Fuel and Materials Laboratory China (Grant No. STRFKL-2013-05) and the 56th China Postdoctoral Science Foundation (Grant No. 2014M560980).

References

[1] F. Lefebvre, C. Lemaignan, Irradiation effects on corrosion of zirconium alloy claddings, J. Nucl. Mater. 248 (1997) 268–274.
[2] B. Cox, C. Wu, Transient effects of lithium hydroxide and boric-acid on zircaloy corrosion, J. Nucl. Mater. 224 (1995) 169–178.
[3] J.-J. Gu, Y.-H. Ling, R.-Q. Zhang, X. Dai, X.-D. Bai, Properties of passive nano films on zircaloy-4 affected by defects induced by hydrogen permeation, Chin. Phys. B 23 (2014) 088106.
[4] B. Cox, Y.M. Wong, A hydrogen uptake micro-mechanism for Zr alloys, J. Nucl. Mater. 270 (1999) 134–146.
[5] B. Cox, Some thoughts on the mechanisms of in-reactor corrosion of zirconium alloys, J. Nucl. Mater. 336 (2005) 331–368.
[6] Q.W. Knapp, J.C. Wren, Film formation on type-316L stainless steel as a function of potential: Probing the role of gamma-radiation, Electrochim. Acta 80 (2012) 90–99.
[7] Y. Nishino, M. Endo, E. Ibe, T. Yasuda, Formation and dissolution of oxide film on zirconium alloys in 288 degrees C pure water under gamma-ray irradiation, J. Nucl. Mater. 248 (1997) 292–298.
[8] Y. Etoh, S. Shimada, M. Sasaki, T. Kogai, H. Hayashi, M. Kitamura, K. Tsuji, M. Yamawaki, Study of environmental effects on water-side corrosion of Zircaloy-2 fuel cladding, J. Nucl. Mater. 248 (1997) 299–305.
[9] M. Behazin, J.J. Noel, J.C. Wren, Combined effects of pH and gamma-irradiation on the corrosion of Co-Cr alloy stellite-6, Electrochim. Acta 134 (2014) 399–410.
[10] T. Motooka, A. Komatsu, T. Tsukada, M. Yamamoto, Effect of gamma radiolysis on pit initiation of zircaloy-2 in water containing sea salt, J. Nucl. Sci. Technol. 51 (2014) 987–995.
[11] K. Daub, X. Zhang, J.J. Noel, J.C. Wren, Gamma-radiation-induced corrosion of carbon steel in neutral and mildly basic water at 150 degrees C, Corros. Sci. 53 (2011) 11–16.
[12] H. Akhiani, J.A. Szpunar, Effect of surface roughness on the texture and oxidation behavior of Zircaloy-4 cladding tube, Appl. Surf. Sci. 285 (2013) 832–839.
[13] X. Wu, Y. Ling, L. Liu, Z. Huang, Enhanced photoelectrocatalytic degradation of methylene blue on smooth TiO[sub 2] nanotube array and its impedance analysis, J. Electrochem. Soc. 156 (2009) K65.
[14] D.Q. Peng, X.D. Bai, X.W. Chen, Q.G. Zhou, X.Y. Liu, R.H. Yu, Comparison of electrochemical behavior of zirconium and zircaloy-4 implanted with Y and Ce ions, Appl. Surf. Sci. 221 (2004) 259–271.
[15] P. Barberis, A. Frichet, Characterization of Zircaloy-4 oxide layers by impedance spectroscopy, J. Nucl. Mater. 273 (1999) 182–191.
[16] O. Gebhardt, A. Hermann, Microscopic and electrochemical impedance spectroscopy analyses of Zircaloy oxide films formed in highly concentrated L1OH solution, Electrochim. Acta 41 (1996) 1181–1190.
[17] D.M. Rishel, K.L. Eklund, B.F. Kammenzind, In situ EIS measurements of irradiated zircaloy-4 post-transition corrosion kinetic behavior, Am. Soc. Test Mater. 1505 (2009) 326–359.
[18] Y. Chen, M. Urquidi-Macdonald, D.D. Macdonald, The electrochemistry of zirconium in aqueous solutions at elevated temperatures and pressures, J. Nucl. Mater. 348 (2006) 133–147.
[19] N.A.P. Kiran Kumar, J.A. Szpunar, EBSD studies on microstructure and crystallographic orientation of δ-hydrides in Zircaloy-4, Zr–1% Nb and Zr–2.5% Nb, Mater. Sci. Eng. A 528 (2011) 6366–6374.
[20] Y. Nishino, A.R. Krauss, Y.P. Lin, D.M. Gruen, Initial oxidation of zirconium and Zircaloy-2 with oxygen and water vapor at room temperature, J. Nucl. Mater. 228 (1996) 346–353.
[21] H. Akhiani, A. Hunt, X. Cui, A. Moewes, J. Szpunar, The electronic structure of zirconium in hydrided and oxidized states, J. Alloys Compd. 622 (2015) 463–470.
[22] J.D. Corbett, H.S. Marek, A photoelectron spectroscopic study of the zirconium monohalide hydrides and zirconium dihydride - classification of metal-hydrides as conventional compounds, Inorg. Chem. 22 (1983) 3194–3202.
[23] X. Wang, X. Zeng, G. Wu, S. Yao, Y. Lai, Effects of tantalum ion implantation on the corrosion behavior of AZ31 magnesium alloys, J. Alloys Compd. 437 (2007) 87–92.
[24] D.J. Park, J.Y. Park, Y.H. Jeong, Microstructural analysis and XPS investigation of nodular oxides formed on Zircaloy-4, J. Nucl. Mater. 412 (2011) 233–238.
[25] W. Chen, L. Wang, S. Lu, Influence of oxide layer on hydrogen desorption from zirconium hydride, J. Alloys Compd. 469 (2009) 142–145.
[26] J. Li, X. Bai, D. Zhang, H. Li, Characterization and structure study of the anodic oxide film on Zircaloy-4 synthesized using NaOH electrolytes at room temperature, Appl. Surf. Sci. 252 (2006) 7436–7441.
[27] W.G. Burns, P.B. Moore, Water radiolysis and its effect upon in-reactor zircaloy corrosion, Radiat. Eff. Defects Solids 30 (2006) 233–242.
[28] J.M. Joseph, B.S. Choi, P. Yakabuskie, J.C. Wren, A combined experimental and model analysis on the effect of pH and O-2(aq) on gamma-radiolytically produced H-2 and H_2O_2, Radiat. Phys. Chem. 77 (2008) 1009–1020.